

11-9-2018

CFD Modeling on Hydrodynamic Characteristics of Multiphase Counter-Current Flow in a Structured Packed Bed for Post-Combustion CO₂ Capture

Li Yang

China University of Mining and Technology, China

Fang Liu

China University of Mining and Technology, China

Kozo Saito

University of Kentucky, ksaito@uky.edu

Kunlei Liu

University of Kentucky, kunlei.liu@uky.edu

Right click to open a feedback form in a new tab to let us know how this document benefits you.

Follow this and additional works at: https://uknowledge.uky.edu/me_facpub

 Part of the [Mechanical Engineering Commons](#), and the [Power and Energy Commons](#)

Repository Citation

Yang, Li; Liu, Fang; Saito, Kozo; and Liu, Kunlei, "CFD Modeling on Hydrodynamic Characteristics of Multiphase Counter-Current Flow in a Structured Packed Bed for Post-Combustion CO₂ Capture" (2018). *Mechanical Engineering Faculty Publications*. 54.

https://uknowledge.uky.edu/me_facpub/54

This Article is brought to you for free and open access by the Mechanical Engineering at UKnowledge. It has been accepted for inclusion in Mechanical Engineering Faculty Publications by an authorized administrator of UKnowledge. For more information, please contact UKnowledge@lsv.uky.edu.

CFD Modeling on Hydrodynamic Characteristics of Multiphase Counter-Current Flow in a Structured Packed Bed for Post-Combustion CO₂ Capture

Notes/Citation Information

Published in *Energies*, v. 11, issue 11, 3103, p. 1-14.

© 2018 by the authors. Licensee MDPI, Basel, Switzerland.

This article is an open access article distributed under the terms and conditions of the Creative Commons Attribution (CC BY) license (<http://creativecommons.org/licenses/by/4.0/>).

Digital Object Identifier (DOI)

<https://doi.org/10.3390/en11113103>

Article

CFD Modeling on Hydrodynamic Characteristics of Multiphase Counter-Current Flow in a Structured Packed Bed for Post-Combustion CO₂ Capture

Li Yang ^{1,2}, Fang Liu ^{1,2,*} , Kozo Saito ³ and Kunlei Liu ^{3,4,*}

¹ Key Laboratory of Coal-Based CO₂ Capture and Geological Storage, China University of Mining and Technology, Xuzhou 221116, Jiangsu, China; li.yang@cumt.edu.cn

² School of Electrical and Power Engineering, China University of Mining and Technology, Xuzhou 221116, Jiangsu, China

³ Department of Mechanical Engineering, College of Engineering, University of Kentucky, Lexington, KY 40506, USA; ksaito@uky.edu

⁴ Center for Applied Energy Research, University of Kentucky, Lexington, KY 40511, USA

* Correspondence: fang.liu@cumt.edu.cn (F.L.); kunlei.liu@uky.edu (K.L.)

Received: 28 September 2018; Accepted: 7 November 2018; Published: 9 November 2018



Abstract: Solvent-based post combustion CO₂ capture is a promising technology for industrial application. Gas-liquid interfaces and interactions in the packed bed are considered one of the key factors affecting the overall CO₂ absorption rate. Understanding the hydrodynamic characterizations within packed beds is essential to identify the appropriate enhanced mass transfer technique. However, multiphase counter-current flows in the structured packing typically used in these processes are complicated to visualize and optimize experimentally. In this paper, we aim to develop a comprehensive 3D multiphase, counter-current flow model to study the liquid/gas behavior on the surface of structured packing. The output from computational fluid dynamics (CFD) clearly visualized the hydrodynamic characterizations, such as the liquid distributions, wettability, and film thicknesses, in the confined packed bed. When the liquid *We* (Weber number) was greater than 2.21, the channel flow became insignificant and flow streams became more disorganized with more droplets at larger sizes. The portion of dead zones is decreased at higher liquid *We*, but it cannot be completely eliminated. Average film thickness was about 0.6–0.7 mm, however, its height varied significantly.

Keywords: CO₂ capture; structured packing; CFD modeling; multiphase counter-current flow; hydrodynamics

1. Introduction

Scientific consensus exists that the primary driving mechanism for global warming is the global increases in atmospheric carbon dioxide (CO₂) concentrations, which is attributed to the anthropogenic emissions from the use of fossil fuels, and the use of coal alone accounted for 43% of global CO₂ emissions [1]. Post-combustion CO₂ capture using solvent-based CO₂ absorption technologies is one of the most promising approaches among the current CO₂ capture technologies and may be implemented at the large-scale in power generation [2]. A schematic diagram of a solvent-based CO₂ absorption process is presented in Figure 1. It includes an absorber, a stripper, and their necessary auxiliary equipment for an aqueous solvent circulating between the two reactors [3]. Both reactors typically use a packed bed to improve the mass transfer by providing an effective contact area between gas and liquid phase reactants [4] due to relatively slow reaction kinetics. The packing materials are in many different forms, but they can be generally divided into random and structured packing. The structured

packing can provide a similar effective surface area but much less pressure drop compared to random packing, making it a good candidate for application in post-combustion CO₂ capture processing, and is investigated herein [5].

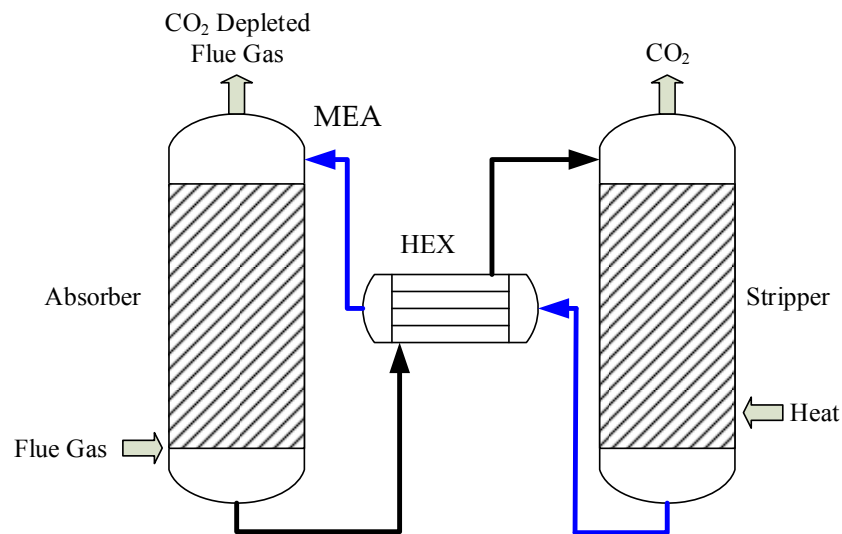


Figure 1. Schematic diagram of a post combustion solvent-based CO₂ capture process. MEA means monoethanolamine; HEX means heat exchanger.

The absorber is expected to be very large and could make up approximately 20% of the capital cost required for CO₂ capture. For example, a CO₂ absorber capable of handling 90% capture of CO₂ from a 0.7 MWe power system would be approximately 19.5 m in height and have at least 13.7 m of structure packing [6,7]. Therefore, understanding the hydrodynamic characterizations within packed beds is of the essence, which will provide insights for gas/liquid mixing enhancement, channel flow prevention, and surface wettability estimation, and then develop techniques to enhance the mass transfer by intensifying the gas/liquid contact and mixing.

Extensive investigations on macro-scale performance have been performed on packed bed reactors over the years [8–10], however, the experimental study on micro-scale hydraulics on the packing surface is scarce. Because, experimentally, it is almost impossible to insert measuring devices to determine the wettability, gas/liquid contact interface, or fluid pattern due to limited available space. Alternatively, with applications of supercomputing, computational fluid dynamics (CFD) has become a possible tool for studying multiphase flows with complicated and relative large geometries [11,12]. Also, overall process performance and individual modifications can be easily evaluated, and test data can be better understood with the aid of such process modeling. Recently, researchers built a 3D numerical model to study the hydrodynamic characterizations, in which the geometry selected was mono-sized, spherical particles were arranged in a cylindrical container [13,14] or inclined or flat plates [15], and the flow was chosen for co-current, or counter-current gas-liquid flows. In contrast, CO₂ absorption processes are typically two-phase counter-current unstable flow, and current simulations are insufficient to provide a clear understanding of the dependencies for their 3D hydrodynamics in structured packing. In order to reduce computing complexity, researchers [6,16] used a porous media zone to simulate structured packing. This method could provide certain information in the simulation and design of new geometries. However, it cannot precisely present the interactions between the two phases under counter-current flow. Thus, no information can be acquired to enhance the gas/liquid mixing. Table 1 lists representative CFD models in structured-packing bed hydrodynamic study.

Table 1. Computational fluid dynamics (CFD) models in structured-packing bed hydrodynamic study.

Reference	Geometry Models	Contribution
Yu et al. (2018) [17]	2D Structured and 3D Porous Model	From the 2D volume of fluid (VOF) model, the accumulation of the liquid in the troughs of the rough surface caused the average film thickness to be larger on the rough surface than on the smooth surface, particularly for low liquid loads. In the 3D VOF model, the flow paths were similar on the two surfaces, but the effective wetted area was slightly larger on the rough surface than on the smooth surface.
Olenberg et al. (2017) [18]	Montz B1-250 Structured Model	Built a single-phase CFD simulation model, and predicted the pressure drop in structured packings.
Haroun et al. (2014) [19]	3-D Vertical Plate Model	Prediction of effective area and liquid hold-up in structured packings.
Ding et al. (2015) [20]	3D Structured Model	Characterized the pressure drop trend.
Fourati et al. (2013) [21]	1D Model	The Eulerian two-fluid framework with user-defined functions and associated models are taken into account in the liquid dispersion model.
Haroun et al. (2012) [22]	2-D Structured Packing Model	Studied mass transfer and liquid hold-up in a 2D cross section structured packing using the VOF method.

A key approach missing for a 3D model to assess post combustion CO₂ capture reactions is to build a true packing geometry instead of a porous media configuration, and consider the solvent properties along the packing length. In this study, a 3D CFD model will be built to understand the hydraulic characterizations in the structured bed, and to provide insights to estimate the surface wettability, prevent the channel flow, and identify the way to enhance the gas/liquid mixing. These results expand the CFD model for efficient industrial application.

2. Computational Model

2.1. Governing Equations

The multi-fluid CFD volume of fluid (VOF) model is applied in this work. It has been considered as suitable to describe the flow characterization, especially for simulating liquid break-up and the interaction of two phases, and has been successfully implemented in other applications [23,24]. It is a surface-tracking technique developed for two or more immiscible fluids where the position of the interface between the fluids is of interest [22]. In the model, a single set of momentum equations is shared by the fluids, and the volume fraction of each fluid in each computational cell is tracked throughout the domain. By solving the governing equations, the phasic volume fraction, a concept describing the volume fraction of gas and liquid, can be determined [25]. The governing equations of the two-phase flow are given as:

Continuity equation

$$\frac{\partial \rho}{\partial t} + \nabla \cdot (\rho \vec{v}) = 0 \quad (1)$$

Momentum equation

$$\frac{\partial}{\partial t} (\rho \vec{v}) + \nabla (\rho \vec{v} \vec{v}) = -\nabla p + \nabla \left[\mu \left(\nabla \vec{v} + \nabla \vec{v}^T \right) \right] + \rho \vec{g} + \vec{F} \quad (2)$$

where $\vec{v} = \frac{a_1 \rho_1 \vec{v}_1 + a_2 \rho_2 \vec{v}_2}{\rho}$, \vec{F} is the interface drag force.

Each phase's volume fraction is a_k , where:

$$\sum_{k=1}^n a_k = 1. \quad (3)$$

For a two-phase system:

$$\rho = a_2 \rho_L + (1 - a_2) \rho_G \quad (4)$$

$$\mu = a_2\mu_L + (1 - a_2)\mu_G \quad (5)$$

where a_k ranges from 0 to 1; a zero corresponds to a cell filled with the gas phase and a value of one corresponds to a cell filled with the liquid phase. Also, surface tension was represented by the drag force term in Equation (2), and the surface tension model [26] is governed by:

$$\vec{F} = \sigma \frac{\rho k \nabla a_k}{0.5(\rho_L + \rho_G)} \quad (6)$$

where k is the free surface curvature, which is defined as

$$k = \nabla \cdot \hat{n} = \frac{1}{|n|} \left[\left(\frac{n}{|n|} \cdot \nabla \right) |n| - (\nabla \cdot n) \right]. \quad (7)$$

The symbol \hat{n} is a unit normal vector, and $n = \nabla a_k$.

2.2. Geometry

In this manuscript, the Mellapak 250 Y (Sulzer) is selected due to its thorough characterization by many research groups [27]. It is the most popular packing type for various solvents, which has been quoted frequently within the literature on CO₂ absorber processes [28]; the number 250 in its designation indicates a specific surface area of 250 m² m⁻³ and the symbol Y means a surface inclined angle of 45° relative to the flow direction. Mellapak 250 Y is made of corrugated metal sheets arranged side-by-side with opposing channel orientations, as illustrated in Figure 2a,b. To save computational time, one slice was chosen as the modeling geometry, thus, a “sandwich-like” packing was built, as shown in Figure 2c.

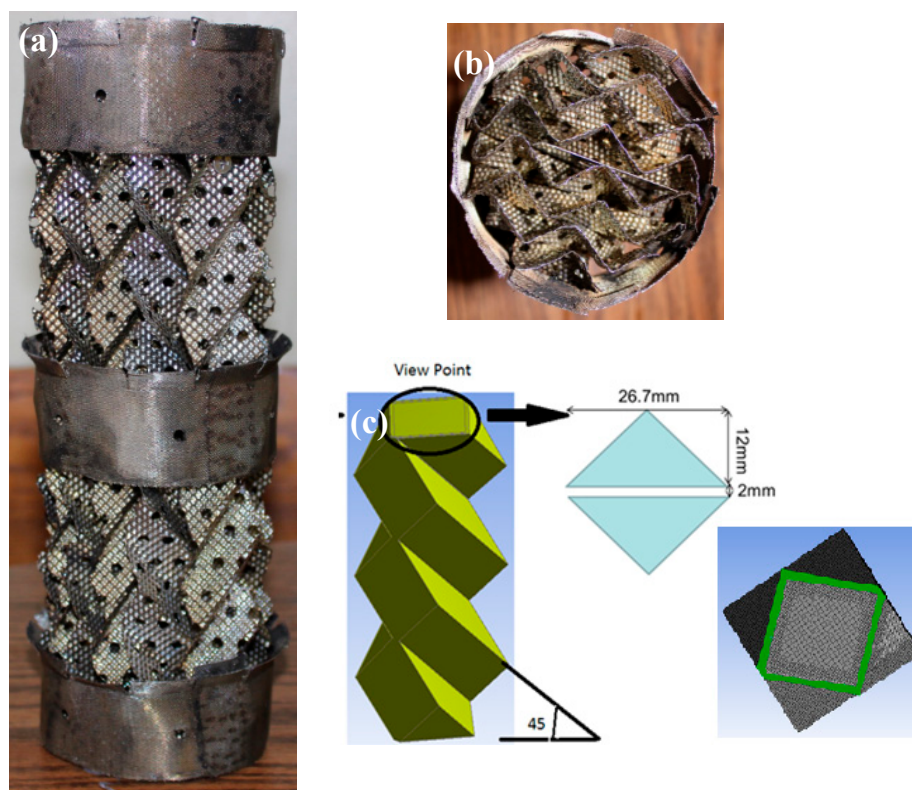


Figure 2. Images of the Mellapak 250 Y structured packing within a bed: (a) overview; (b) top view; and (c) the geometric model.

2.3. Meshing

The mesh independent test was performed at the very beginning of the study. Three different cells of 320,486, 370,804, and 401,038 were applied and compared, and the mesh elements of greater than 320,486 yield similar pressure drops. Typically, larger number of meshes give more accurate results, with fine mesh close to solid surfaces for an accurate determination of the liquid-film thickness, and coarser away from these surfaces; the mesh elements for the study were finally changed to 370,804, as shown in Figure 3. Details of the mesh structure are also provided in Figure 3.

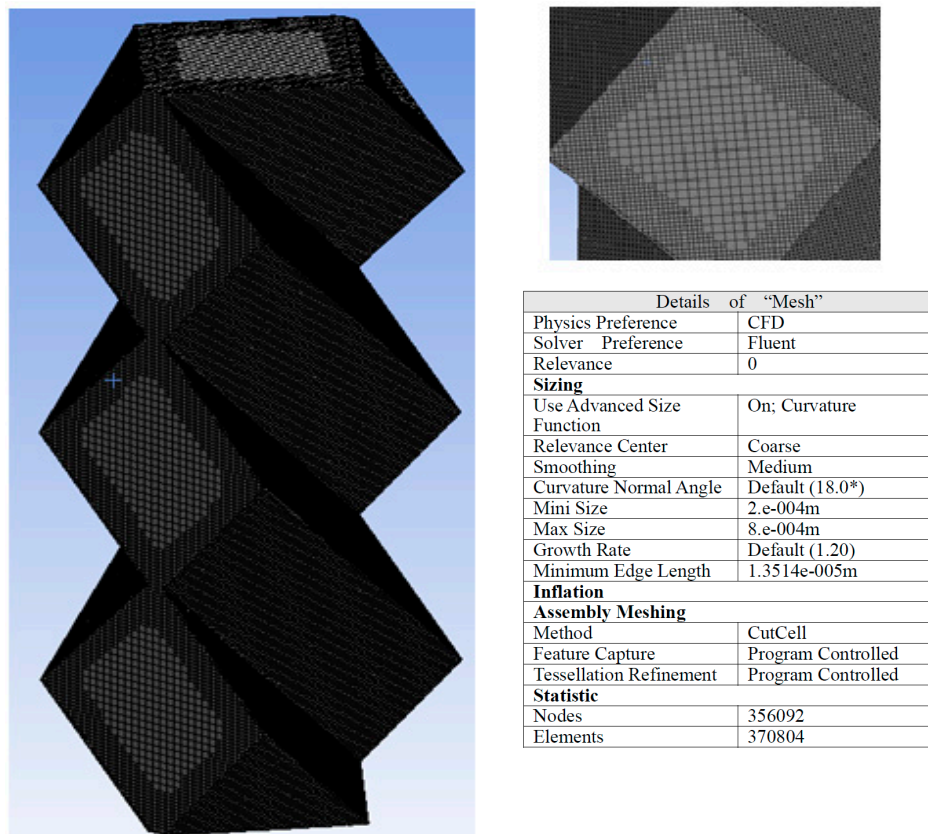


Figure 3. Mesh model and the details of the mesh.

2.4. Turbulence Model

In packed bed flows, the value of Reynolds number, which is generally used to separate laminar or turbulent flows, is different with traditional macroscopic flows [29], in which for $1 < Re$, the flow was dominated by viscous force; for $1 < Re < 150$, the flow was a steady laminar inertial flow; for $150 \leq Re$, the flow was unsteady, chaotic, and qualitatively resembled turbulent flow. In this simulation process, with the range of flow at a minimum of 180 and maximum of 1100, this is turbulence flow. The LES (Large Eddy Simulation) turbulent model was applied, which is popular for use in turbulent flow simulations, and it emphasizes the interactions between phases [5].

The Reynolds number has been calculated as:

$$Re = \frac{\rho v d}{\mu} \quad (8)$$

where the characteristic length d is the thickness of the phase inlet, ρ is the density of the fluid (kg/m^3), v is its velocity (m/s), and μ is the viscosity ($\text{kg}/\text{m}\cdot\text{s}$).

2.5. Boundary Conditions

In the simulation of flow parameters, the velocity-inlet condition was used, the volume fraction of liquid phase was set to 1, and the whole flow field was initially filled with air. To make counter-current flow, the liquid entered from the top and flowed out from the bottom, while gas entered from the bottom and flowed out from the top; to make the liquid continuously flow down the “sandwich-like” packed column, the side walls were set as symmetric boundaries. The schematic overview of flow directions is shown in Figure 4.

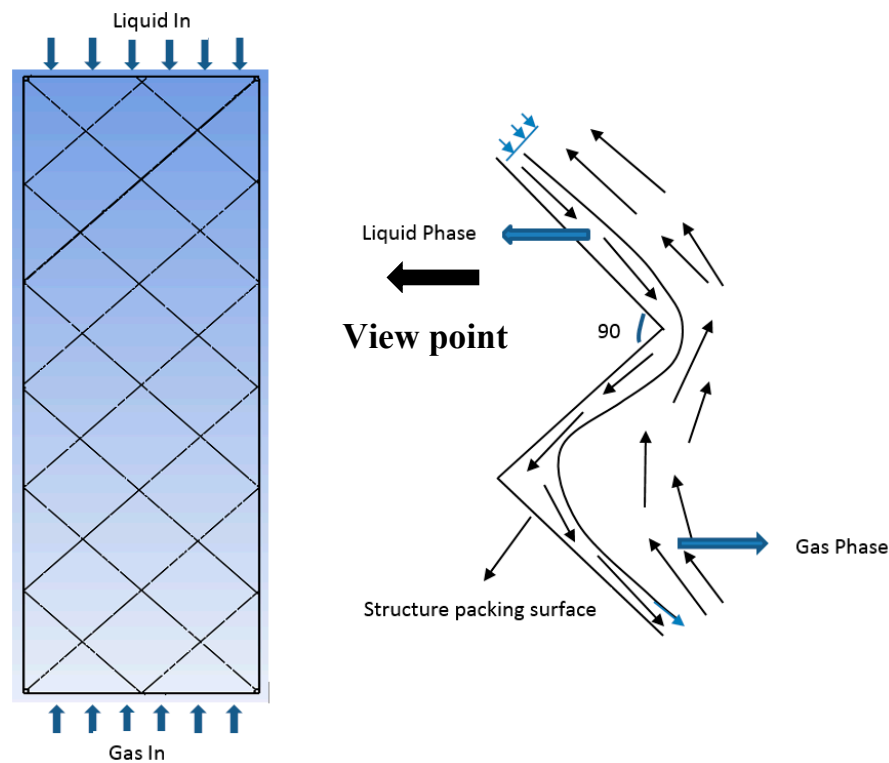


Figure 4. Schematic overview of flow directions.

The Geo-Reconstruct algorithm method was used for interface reconstruction of the volume fraction, a simple scheme for the pressure-velocity coupling. For spatial discretization, the least squares cell-based method was used for the gradient in the spatial discretization set up, the PRESTO method was used for pressure, the second-order upwind method was used for the momentum equation, and the first-order implicit method was used for the transient formulation. The simulation used a transient state to observe the growth of the liquid film and the development of gas–liquid interactions. The time step size for this model was 0.00005 s while solving a maximum 30 iterations per time step. The total computation time for each case was close to 120 h. Table 2 shows the details of boundary conditions for the simulations.

Table 2. Details of boundary conditions of all simulations.

Boundary	Materials	Type	Value	Velocity	Reynolds Number	Weber Number
Liquid inlet	Water	Mass Flow Rate	12.2–48.8 $\text{m}^3/(\text{m}^2\cdot\text{h})$	0.015–0.6 m/s	15–600	0.02–5.13
Gas inlet	Air	Velocity m/s	0.5–1.1 m/s	0.5–1.1 m/s	325–1200	-
Liquid outlet	-	Pressure-outlet	0 Pa	-	-	-
Gas outlet	-	Pressure-outlet	0 Pa	-	-	-

3. Results and Discussion

3.1. Validation of Simulation Model

Liquid holdups and pressure drops from simulation and experiments for the packing bed were compared in Figure 5 and identify whether any parameters can be improved. Experimental values of liquid holdup and pressure drop were obtained by well-developed empirical models for a structured packing published by Stichlmair [30]; it is outlined by Equation (9) and has the Ergun equation [31] as its foundation after modification to account for the presence of a liquid.

$$\frac{\Delta P}{l} = \frac{3}{4f'_0 \left[\frac{1-\varepsilon'}{e^{4.65}} \right] \rho_G U_G^2} / d'_p \quad (9)$$

where $f'_0 = f_0 \left\{ \left[1 - \varepsilon \left(1 - \frac{h_0}{\varepsilon} \right) \right] / (1 - \varepsilon) \right\}^{c/3}$, ρ_G is gas density, U_G is gas velocity.

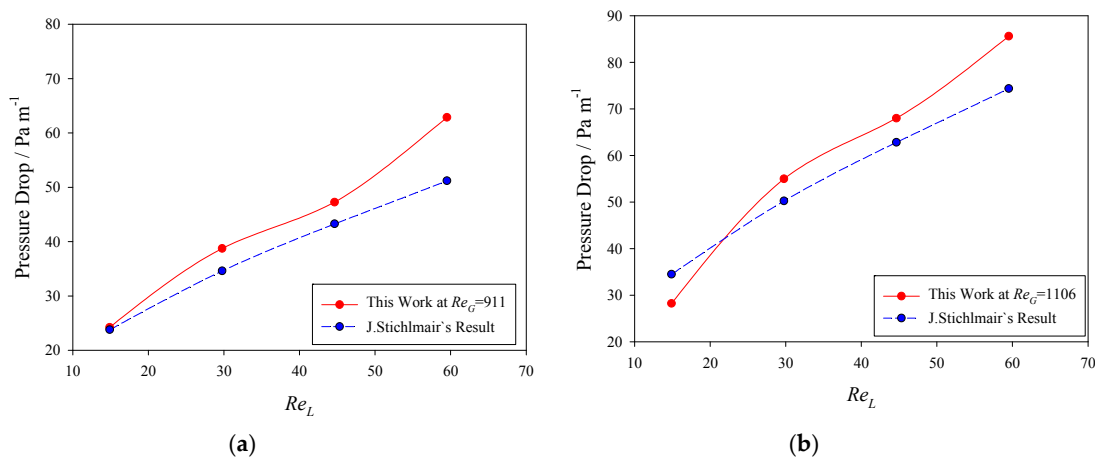


Figure 5. A comparison of pressure drops from Stichlmair's empirical model and the CFD simulation results for different gas flow rates: (a) $Re_G = 911$, (b) $Re_G = 1106$.

$f_0 = \frac{C_1}{Re_G} + \frac{C_2}{Re_G^{1/2}} + C_3$, in this type packing, $C_1 = 5$, $C_2 = 3$, $C_3 = 0.45$

$$\varepsilon' = \varepsilon \left(1 - \frac{h}{\varepsilon} \right) \quad (10)$$

$$c = \frac{\left[-\frac{C_1}{Re_G} - \frac{C_2}{2Re_G^{1/2}} \right]}{f_0} \quad (11)$$

$$d'_p = d_p \left\{ \left[1 - \varepsilon \left(1 - \frac{h}{\varepsilon} \right) \right] / (1 - \varepsilon) \right\}^{1/3} \quad (12)$$

$$d_p = 6(1 - \varepsilon) / a \quad (13)$$

Figure 5a,b show a comparison of gas phase pressure drops as obtained from the empirical model [30] and from the current CFD simulations. As can be seen, pressure drops from both the empirical model and the CFD simulation agreed quite well, increasing monotonically with increased liquid flow rates and gas flow rates.

An empirical relationship for predicting liquid holdup was developed by Billet [32]; it is expressed as:

$$h_0 = 0.555 \left(U_L^2 \frac{a}{g e^{4.65}} \right)^{1/3} \quad (14)$$

where U_L is the liquid velocity in m/s, a is the specific surface area in $\text{m}^2 \text{m}^{-3}$, g is the gravity in m/s^{-2} , and ε is the void fraction in %. Liquid holdups using the developed CFD model at low liquid flow rates and three different gas flow rates were compared to this empirical equation as presented in Figure 6 and show that different gas flow rates had only a very weak effect on liquid holdup, a result consistent with data from the empirical model. Such a weak dependency on gas flow rates may be a result of the liquid film becoming thinner as the gas flow rates were increased. As a consequence of the agreement between the 3D simulations and empirical model results, the CFD model for structured packing was considered validated.

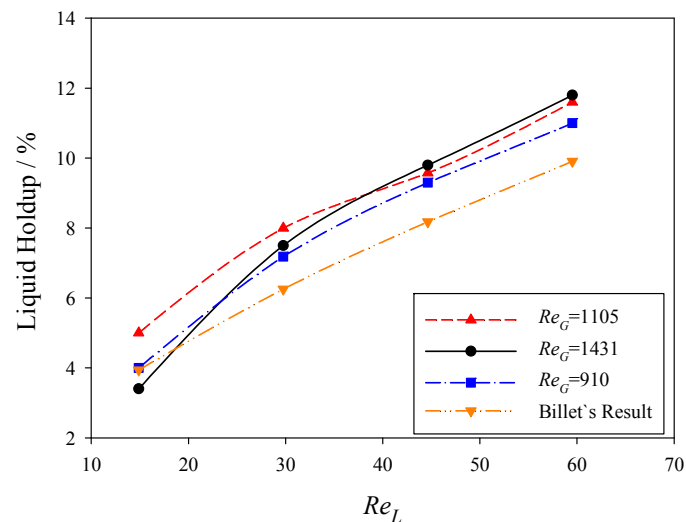


Figure 6. Comparison of liquid holdups from CFD simulations and empirical calculations.

3.2. Liquid Distribution and Surface Wettability

Liquid distributions and their evolution as a function of liquid flow rates were studied. From Figure 7, an interface between the fluids was successfully demonstrated, and especially when strongly curved surfaces are present Weber numbers (We), which are a measure of the relative importance of a fluid's inertia compared to its surface tension, were used as the variable of interest rather than the liquid or gas flow rates [33]. The We number is expressed as:

$$We = \frac{\rho v^2 l}{\sigma} \quad (15)$$

where ρ is the density of the fluid (kg/m^3), v is the fluid velocity (m/s), l is its characteristic length—typically the droplet diameter (m), and σ is the surface tension (N/m) of the liquid.

Three computing outputs were obtained when steady state is achieved at three We numbers. The scale bar on the left shows that a red color represents 100 vol. % liquid and a blue color represents 100 vol. % gas. Since the side walls were set as symmetrized segments, the flow is shown in a rotated orientation and the liquid is shown to continuously flow down the packing surface following a “Z” shape. At low liquid We numbers (e.g., low liquid flow rate), i.e., $We = 0.57$, the liquid flow seemed like a channel flow, and indicated that the packing surface is wetted but interface between liquid and gas is stable. With the increase in liquid We to 2.21, when the inertial forces began to dominate over surface tension, flow streams became more disorganized with more droplets (segment from bulk stream) with larger sizes, indicating an instable and turbulent interaction between gas and liquid, which could benefit channel flow prevention and intensify the gas/liquid mixing to boost the CO_2 capture mass transfer. Further increasing We to 5.13, the flow pattern did not change too much besides increasing the liquid fraction in the packing space compared to $We = 2.21$, resulting in higher pressure drop which

kept on increasing with the increase of gas velocity at this condition, as shown in Figure 8, and implied the potential flooding as demonstrated by the packing operating curve obtained experimentally.

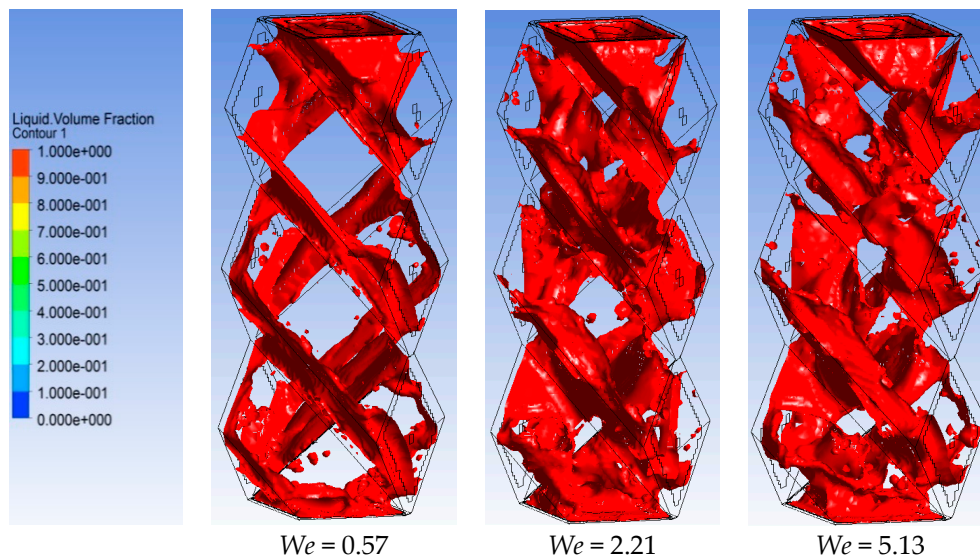


Figure 7. Liquid distribution for structured packing at different liquid We numbers from 0.57 to 5.13 and fixed $Re_G = 1431$.

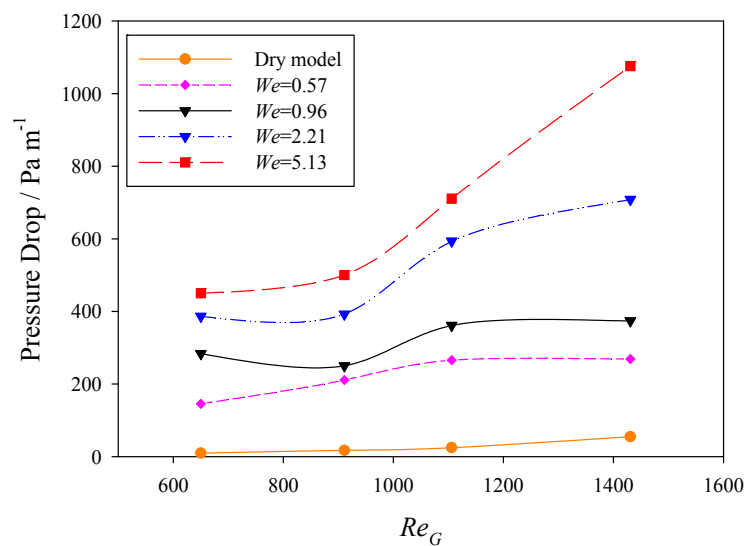


Figure 8. Influence of gas flow rates with fixed liquid velocities on pressure drop.

Figures 9 and 10 show the wettability at different liquid We numbers from 0.57 to 5.13. At $We = 0.57$, the surface of the packing was only partially wetted. Another phenomenon observed was that droplets began to appear near the main flow stream, although the droplet sizes were relatively small. The possible droplet formation mechanisms will be discussed later. Increasing the liquid We number, the coverage of the wetted surface increased significantly. However, the surface was not fully wetted even at $We = 5.13$, which matches the experimental finding—approximately 60–70% of the surface wetted. Those dry surfaces could be referred to as dead zones; in general, as liquid We values increased, the dead zones on the packing surfaces decreased but were not completely eliminated at any We values tested.

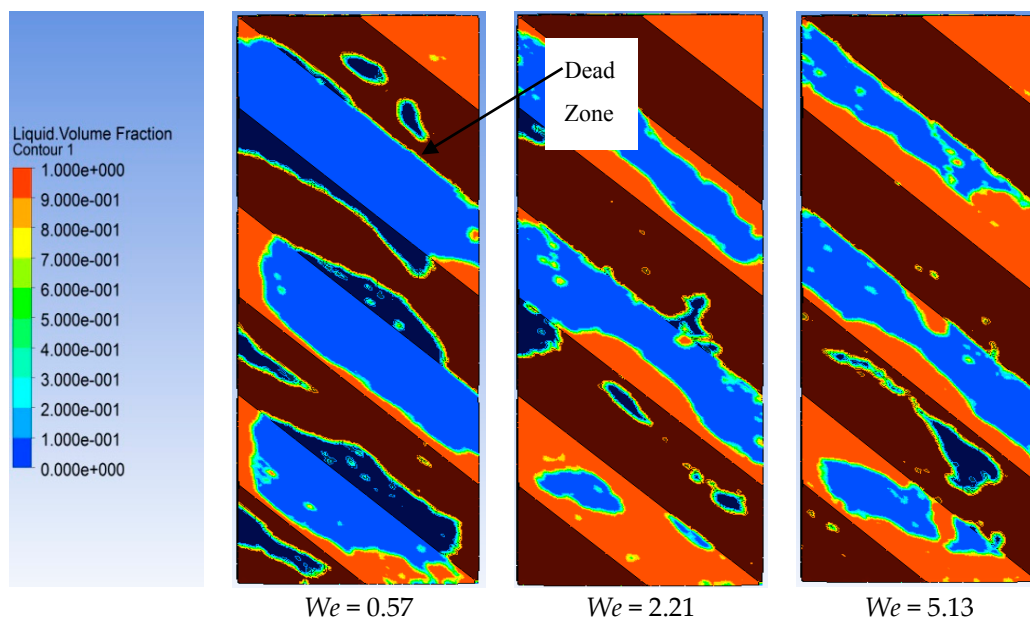


Figure 9. Wettability for structured packing at different liquid We numbers from 0.57 to 5.13 and fixed $Re_G = 1431$.

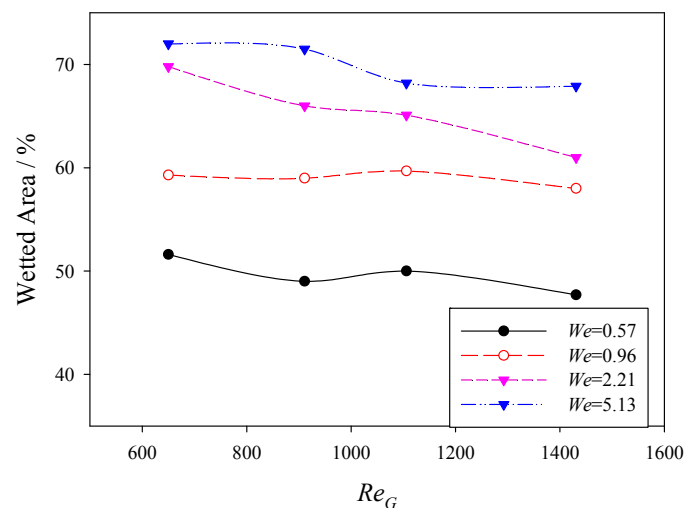


Figure 10. Influence of gas flow rate with fixed liquid flow rate on wetted area.

Interestingly, increasing the gas flow rates only slightly lowered the wetted area at any particular liquid flow rate, which could indicate the lack of impact of the drag force of the gas stream on liquid distribution and fluid. Considering the phenomenon in Figures 7 and 9, at high gas flow rates, it can be anticipated that strong gas–liquid interactions may occur in the structured packing which will increase the mixing of gas and liquid because the curved edges and flow channels help create conditions conducive for gas–liquid interactions; this occurrence may then also lead to the generation of more liquid droplets which can cause decreases in the wetted areas as is observed in Figure 10.

3.3. Formation of Droplets

Figure 11 shows the development of droplets when $Re_G = 1431$ and $We = 5.13$. At $t = 0.011$ s, the liquid reached the packing surface and flowed along its 45° trajectory. At $t = 0.058$ s, the liquid wetted the first element and began to flow onto the second element. Several droplets are seen to have been formed at $t = 0.058$ s at the frontier of the flow stream and turning point of the two packing elements; the area of the neck is smaller than above or below it and, as a consequence, the gas flow velocity is

higher in the neck. By $t = 0.134$ s, the second element had been wetted, and by $t = 0.232$ s the liquid had flowed throughout the whole domain; droplets can be found in every element region by $t = 0.232$ s.

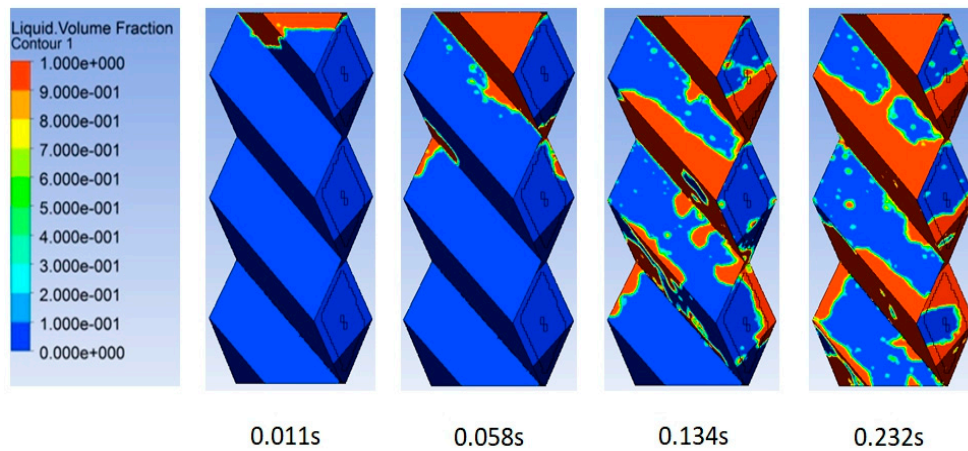


Figure 11. Flow development with time at $Re_G = 1431$ and $We = 5.13$ (red color represents 100 vol. % of liquid and blue color represents 100 vol. % of gas).

Gas and liquid velocity vectors were also monitored to provide insight into gas–liquid interactions in the packed bed, as shown in Figure 12. Downward pointing arrows associate with the direction and velocities of liquid flows, and upward pointing arrows associate with the direction and velocities of gas flows. The gas phase always had higher velocity than the liquid phase and, in general, the liquid flowed along the surface of the packing. However, at turning areas between the sections, the gas and liquid velocity vectors were not parallel to the packing channels. Rather, the gas velocities were shifted away from being parallel to the channels, flowing upwards instead of downwards, and this shift disturbed the liquid flow. Reversed gas flow velocity along with the increased gas velocities in the neck areas can more readily cause the formation of droplets. As droplets develop, the intimacy of gas–liquid interactions increases. Thereby this type of structured packing will also increase the interaction of gas and liquid. Furthermore, the disturbed liquid flow may lead to a less uniform distribution of film thickness.

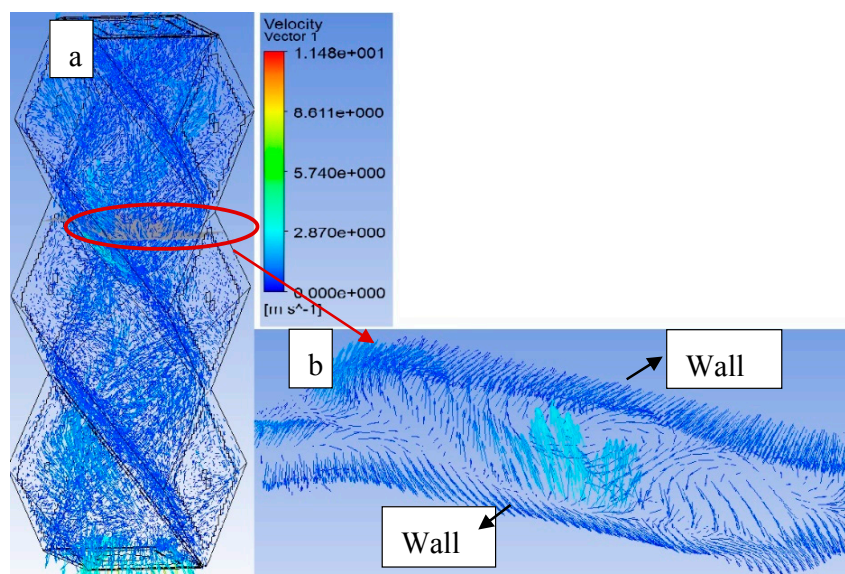


Figure 12. Gas and liquid flow vectors at $Re_G = 1431$ and $We = 5.13$. (a) The velocity vectors in the whole domain. (b) Velocity vectors in a neck area or element channel within the packing.

3.4. Film Thickness

The average film thickness in the packed bed was evaluated by liquid holdup divided by wetted surface area [34]. Figure 13 shows images of the development of film thickness under different liquid We values at constant $Re_G = 1431$. When We was below 2.21, the packing surface was not fully wetted and the film thickness was not uniform; this result indicated that surface tension dominated the liquid flow. When We was increased to 2.21 and beyond, liquid film increased in thickness, and the film thicknesses became more uniform at $We = 2.21$. However, as also shown in Figure 13, the liquid film became less uniform with significant protrusions at $We = 5.13$, which implied strong interactions between the gas and liquid phases. This also implied that the film thickness will be influenced by the time, gas flow rates, and liquid flow rates. However, the average film thickness can be estimated using this model. Figure 14 shows the influence of gas flow rates and liquid flow rates on the average film thickness where film thicknesses were between 0.6–0.7 mm. Larger liquid flow rates created thicker liquid films; for example, the film thickness was near 0.62 mm at $We = 0.57$ and increased to near 0.7 mm when $We = 5.13$. However, changing the gas flow rates had no significant effects or result in any consistent trends to arise on film thickness. However, with increasing gas flow rates, the liquid flow will become unstable.

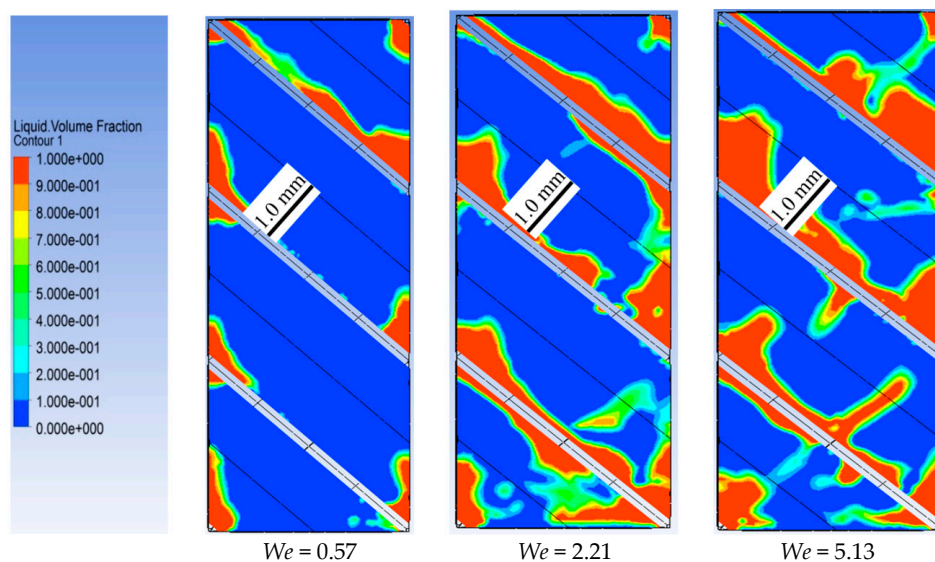


Figure 13. Film thicknesses as a function of liquid flow rates at constant $Re_G = 1431$ (a red color represents 100 vol. % of liquid and blue color is 100 vol. % of gas).

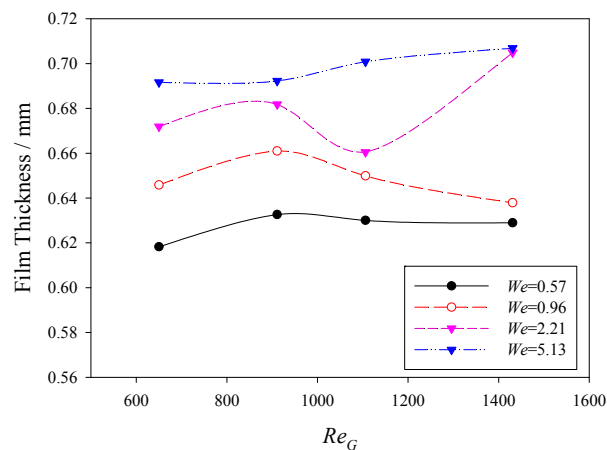


Figure 14. Influence of gas flow rate on film thickness under fixed liquid flow rate.

4. Conclusions

A comprehensive VOF-based 3D CFD model with structured packing in counter-current gas-liquid flow was developed to study the complicated hydrodynamics in the post combustion CO₂ capture process. The model was validated by experimental data in the public domain. The hydrodynamics in a structured packing under various flow conditions were examined and discussed. Inertial forces and surface tension affecting the flow patterns, and a higher *We* number leads to a more uniform liquid distribution, high wettability, and a minimum probability for channel flow. However, a large *We* number (e.g., high liquid flow rate) may lead to flooding. The wetted surface area and average film thickness were greatly affected by the liquid flow rate while slight effects by the gas flow rate were observed. However, increasing the gas flow rate will enhance the gas-liquid interactions, leading to increased liquid film instability and large amount of liquid droplet generation. Average film thickness was about 0.6–0.7 mm. The unparalleled counter flow direction of the gas and liquid is the main reason for droplet formation, where it is more obvious at the turning point of two packing elements.

Author Contributions: Conceptualization, K.L. and K.S.; Methodology, F.L.; Software, L.Y.; Validation, L.Y. and F.L.; Formal Analysis, L.Y. and F.L.; Investigation, L.Y.; Writing-Original Draft Preparation, L.Y.; Writing-Review & Editing, L.Y., F.L., K.L. and K.S.

Funding: This research was funded by the Key Laboratory of Coal-based CO₂ Capture and Geological Storage, Jiangsu Province (China University of Mining and Technology) (NO: 2017A02.), and by the Natural Science Foundation of Jiangsu Province (BK20180645), the author also thanks the support from the Key Project of Scientific Research Frontiers of CUMT (2017XKZD02).

Conflicts of Interest: The authors declare no conflict of interest.

References

1. Yu, H. Carbon capture and storage: A challenging approach for mitigation of global warming. *Int. J. Clean Coal Energy* **2013**, *2*, 23–24. [[CrossRef](#)]
2. Thompson, J.G.; Combs, M.; Abad, K.; Bhatnagar, S.; Pelgen, J.; Beaudry, M.; Rochelle, G.; Hume, S.; Link, D.; Figueroa, J.; et al. Pilot testing of a heat integrated 0.7 MWe CO₂ capture system with two-stage air-stripping: Emission. *Int. J. Greenh. Gas Control* **2017**, *64*, 267–275. [[CrossRef](#)]
3. Yang, L.; Liu, F.; Song, Z.; Liu, K.; Saito, K. 3D Numerical Study of Multiphase Counter-Current Flow within a Packed Bed for Post Combustion Carbon Dioxide Capture. *Energies* **2018**, *11*, 1441. [[CrossRef](#)]
4. Ranade, V.; Chaudhari, R.; Gunjal, P. Hydrodynamics and Flow Regimes. In *Trickle Bed Reactors*; Elsevier: Amsterdam, The Netherlands, 2011; Chapter 2; pp. 25–75.
5. Haroun, Y.; Legendre, D.; Raynal, L. Direct numerical simulation of reactive absorption in gas-liquid flow on structured packing using interface capturing method. *Chem. Eng. Sci.* **2010**, *65*, 351–356. [[CrossRef](#)]
6. Kim, J.; Pham, D.A.; Lim, Y.-I. Gas-liquid multiphase computational fluid dynamics (cfd) of amine absorption column with structured-packing for CO₂ capture. *Comput. Chem. Eng.* **2016**, *88*, 39–49. [[CrossRef](#)]
7. Saito, K.; Ito, A.; Nakamura, Y. Progress in Scale Modeling. In *The International Symposia on Scale Modeling, ISSM VI (2009) and ISSM VII (2013)*; Springer: Berlin, Germany, 2013; Volume II.
8. Pangarkar, K.; Schildhauer, T.; Ommen, J.; Nijenhuis, J.; Kapteijn, F.; Moulijn, J.A. Structured Packings for Multiphase Catalytic Reactors. *Ind. Eng. Chem. Res.* **2008**, *47*, 3720–3751. [[CrossRef](#)]
9. Basden, M.; Eldridge, R.B.; Farone, J.; Feng, E.; Hussey, D.S.; Jacobson, D.L. Liquid holdup profiles in structured packing determined via neutron radiography. *Ind. Eng. Chem. Res.* **2013**, *52*, 17263–17269. [[CrossRef](#)]
10. Guo, X.; Sun, Y.; Li, R.; Yang, F. Experimental investigations on temperature variation and inhomogeneity in a packed bed cld reactor of large particles and low aspect ratio. *Chem. Eng. Sci.* **2014**, *107*, 266–276. [[CrossRef](#)]
11. Yeoh, G.; Tu, J. *Computational Techniques for Multiphase Flows*. Butterworth-Heinemann: Oxford, UK, 2010.
12. Zhang, H. High Temperature Flow Solver for Aerothermodynamics Problems. Ph.D. Thesis, University of Kentucky, Lexington, KY, USA, August 2015.
13. Lopes, R.J.G.; Quinta-Ferreira, R.M. Cfd modelling of multiphase flow distribution in trickle beds. *Chem. Eng. J.* **2009**, *147*, 342–355. [[CrossRef](#)]

14. Gunjal, P.; Kashid, M.; Ranade, V.; Chaudhari, R.V. Hydrodynamics of Trickle-Bed Reactors: Experiments and CFD Modeling. *Ind. Eng. Chem. Res.* **2005**, *44*, 6278–6294. [[CrossRef](#)]
15. Wen, X.; Shu, Y.; Nandakumar, K.; Chuang, K.T. Predicting liquid flow profile in randomly packed beds from computer simulation. *AIChE J.* **2001**, *47*, 1770–1779. [[CrossRef](#)]
16. Hoffmann, A.; Ausner, I.; Repke, J.; Wozny, G. Fluid dynamics in multiphase distillation processes in packed towers. *Comput. Chem. Eng.* **2005**, *29*, 1433–1437. [[CrossRef](#)]
17. Yu, D.; Cao, D.; Li, Z.; Li, Q. Experimental and CFD studies on the effects of surface texture on liquid thickness, wetted area and mass transfer in wave-like structured packings. *Chem. Eng. Res. Des.* **2018**, *129*, 170–181. [[CrossRef](#)]
18. Olenberg, A.; Reschetnikb, W.; Kullmer, G.; Kenig, E.Y. Optimization of structured packings using twisted tape inserts. *Chem. Eng. Res. Des.* **2018**, *132*, 1–8. [[CrossRef](#)]
19. Haroun, Y.; Raynal, L.; Alix, P. Prediction of effective area and liquid hold-up in structured packings by cfd. *Chem. Eng. Res. Des.* **2014**, *92*, 2247–2254. [[CrossRef](#)]
20. Ding, H.; Li, J.; Xiang, W.; Liu, C. Cfd simulation and optimization of winpak-based modular catalytic structured packing. *Ind. Eng. Chem. Res.* **2015**, *54*, 2391–2403. [[CrossRef](#)]
21. Fourati, M.; Roig, V.; Raynal, L. Liquid dispersion in packed columns: Experiments and numerical modeling. *Chem. Eng. Sci.* **2013**, *100*, 266–278. [[CrossRef](#)]
22. Haroun, Y.; Raynal, L.; Legendre, D. Mass transfer and liquid hold-up determination in structured packing by cfd. *Chem. Eng. Sci.* **2012**, *75*, 342–348. [[CrossRef](#)]
23. Ginzburg, I.; Wittum, G. Two-phase flows on interface refined grids modeled with vof, staggered finite volumes, and spline interpolants. *J. Comput. Phys.* **2001**, *166*, 302–335. [[CrossRef](#)]
24. Renardy, Y.; Renardy, M. Prost: A parabolic reconstruction of surface tension for the volume-of-fluid method. *J. Comput. Phys.* **2002**, *183*, 400–421. [[CrossRef](#)]
25. Zhang, C.; Zhang, W.; Lin, N.; Tang, Y.; Zhao, C.; Gu, J.; Lin, W.; Chen, X.; Qiu, A. A two-phase flow model coupling with volume of fluid and immersed boundary methods for free surface and moving structure problems. *Ocean Eng.* **2013**, *74*, 107–124. [[CrossRef](#)]
26. Hirt, C.; Nichols, B. Volume of fluid (VOF) method for the dynamics of free boundaries. *J. Comput. Phys.* **1981**, *39*, 201–225. [[CrossRef](#)]
27. Olsson, E.; Kreiss, G. A conservative level set method for two phase flow. *J. Computat. Phys.* **2005**, *210*, 225–246. [[CrossRef](#)]
28. Olujić, Ž.; Seibert, A.; Fair, J. Influence of corrugation geometry on the performance of structured packings: An experimental study. *Chem. Eng. Process. Process Intensif.* **2000**, *39*, 335–342. [[CrossRef](#)]
29. Cable, M. An Evaluation of Turbulence Models for the Numerical Study of Forced and Natural Convective Flow in Atria. Master's Thesis, Queen's University, Kingston, ON, Canada, May 2009.
30. Stikkelman, R.; Teeuw, H.; Wesselingh, H.; de Graauw, J.; Olujić, Z. A study of gas and liquid distributions in structured packings. *Chem. Eng. Technol.* **1989**, *12*, 445–449. [[CrossRef](#)]
31. Ergun, S.; Orning, A.A. Fluid Flow through Randomly Packed Columns and Fluidized Beds. *Ind. Eng. Chem.* **1949**, *41*, 1179–1184. [[CrossRef](#)]
32. Billet, R. *Packed Towers: In Processing and Environmental Technology*; Wiley-VCH: Wernheim, Germany, 1995.
33. Sebastia-Saez, D.; Gu, S.; Ranganathan, P.; Papadikis, K. 3D modeling of hydrodynamics and physical mass transfer characteristics of liquid film flows in structured packing elements. *Int. J. Greenh. Gas Control.* **2013**, *19*, 492–502. [[CrossRef](#)]
34. Jo, D. Hydrodynamic model of interfacial area for trickling flow in a packed bed. *J. Mech. Sci. Technol.* **2016**, *30*, 171–178. [[CrossRef](#)]

